A Numerical Study of Loop Current Eddy Interaction with Topography in the Western Gulf of Mexico

DAVID C. SMITH, IV*

Department of Oceanography, Texas A&M University, College Station, TX 77843

(Manuscript received 30 November 1984, in final form 28 January 1986)

ABSTRACT

Anticyclones originating from the Loop Current are known to propagate into the western Gulf of Mexico. Their frequency of generation, their long lifetimes, and satellite data suggest that at any one time one or more eddies may occupy the Gulf. Given the eddy sizes (100–200 km) and geometric confinement of the Gulf, it would appear that there may be significant interactions of individual eddies and/or interactions of the eddies with bottom topography. These possibilities are explored through the use of a two-layer primitive equation model. Variable parameters in this model study are eddy strength, vertical structure, lateral friction, and initial location relative to topography.

Results indicate that eddy motion is governed by two dyamical regimes depending on its lower layer rotational strength. Anticyclones with significant lower layer anticyclonic structure develop offshore directed self advective tendencies associated with topographic dispersion which induces asymmetry in the eddy. Eddies with weaker lower layer flow rapidly evolve through topographic dispersion to upper layer features and propagate independently of topography, interacting with the coastal boundary. The boundary can also induce eddy asymmetry with resulting alongshore self advection tendencies leading to northward motion for anticyclones along the western boundary.

1. Introduction

The formation of intense rotating eddy features by unstable oceanic jets is now well observed in numerous locations in the world's oceans. The role that these energetic mesoscale features play in the ocean general circulation is thought to be significant but is not fully understood. With the goal of understanding this role, a number of investigations have focused on the dynamics of these features in isolation. The propagation and decay of isolated eddies has been shown to be influenced by size and strength (McWilliams and Flierl, 1979; Smith and Reid, 1982), vertical structure (McWilliams and Flierl, 1979; Mied and Lindemann, 1979), atmospheric forcing (Dewar, 1983), and bottom topography (Smith and O'Brien, 1983). Other factors not considered in previous studies may, however, significantly influence eddy dynamics. The interaction of the isolated features with other strong flows (fronts or eddies) and with lateral boundaries has had less attention. Hence the application of these numerous previous results to a particular physical situation is not always straightforward.

Loop Current eddies with radial scales of approximately 100 km are intense (rotational velocities of order 1 m s^{-1}) anticyclonic vortices. After their formation they propagate westward into the geometrically confined (1000 × 800 km) domain of the western Gulf. The frequency of generation (at least one per year), their large size relative to the Gulf, and their long lifetimes suggest that eddy–eddy interaction may occur. In addition, the small domain in which they are contained may eliminate or induce certain eddy dynamics not seen in isolated open ocean eddies away from boundaries.

A series of numerical experiments designed to determine the response of anticyclonic eddies to topography and the geometry of the western Gulf is presented here. The effect of eddy strength, vertical structure, lateral friction and location relative to topography on eddy motion and decay is examined.

A brief summary of observational data on Loop Current eddies is given in section 2. Section 3 provides information on previous numerical experiments of eddy/topography interaction, followed by (section 4) model description and eddy initial conditions. A summary of previous isolated eddy experiments over flat topography and a more detailed description of model technique used here is provided in Smith and O'Brien (1983). Numerical experiments are discussed in section

* Present address: Department of Oceanography, Naval Postgraduate School, Monterey, CA 93943.

5. Comparison with observations are made in section 6. Appendices A and B contain definitions of terms, summary tables of energy changes and eddy net translation during simulations.

2. Observational data

Loop Current eddies in the Gulf of Mexico result from the barotropically unstable (Hurlburt and Thompson, 1980) meandering of Gulf inflow through the Yucatan Strait. Figure 1 shows this formation process. After their formation in the eastern Gulf, the eddies propagate westward with speeds ranging 2.2 to 4.9 km day^{-1} (Elliot, 1979). The frequency of generation is variable with one per year being a lower limit and as many as three suggested by hydrographic data (Elliot, 1982).

Given the frequency of generation and the long lifetimes of these features within the relatively small geometric confines of the Gulf, one is led to speculate about the fate of any one particular feature. Recent drifter data (Kirwan, et al., 1984) indicates a southwestward path across the deep flat bottom portion of the basin with subsequent northward motion along the Texas continental slope. The occurrence of anticyclonic circulation in the western Gulf has been documented in a number of hydrographic data sets (e.g., see Molinari et al., 1978; Merrell and Morrison, 1981; Merrell and Vasquez, 1983; Brooks and Legeckis, 1982; Brooks, 1983; Brooks, 1984). Using historical temperature and salinity fields, Molinari et al. (1978) estimated seasonal and annual geostrophic transports for the entire Gulf. Their results show anticyclonic motions at all depths to 3000 m for the central and western Gulf. The anticyclonic motion in the upper 500 m in the western Gulf is stronger in the summer and winter. This is consistent with the hypothesis of Sturges and Blaha (1976) that the anticyclonic motion is driven by the wind stress curl over the Gulf which is stronger in those seasons. The location of the anticyclone is quite variable, however, and no conclusive data exists for its behavior as a function of time. By comparing eddy strength for two realizations for a particular eddy, Brooks (1984) estimates a time scale of at least two months associated with eddy decay over the topographic slope in the western Gulf.

In addition to this frequently observed anticyclone in the western Gulf, a semipermanent cyclone to its north also appears to exist. The existence of the cyclone has been attributed to cyclonic vorticity associated with Loop Current formation (Elliot, 1982), wind forcing (Merrell and Vasquez, 1983) and topographic Rossby wave dispersion of the anticyclone on the continental slope (Smith and O'Brien, 1983).

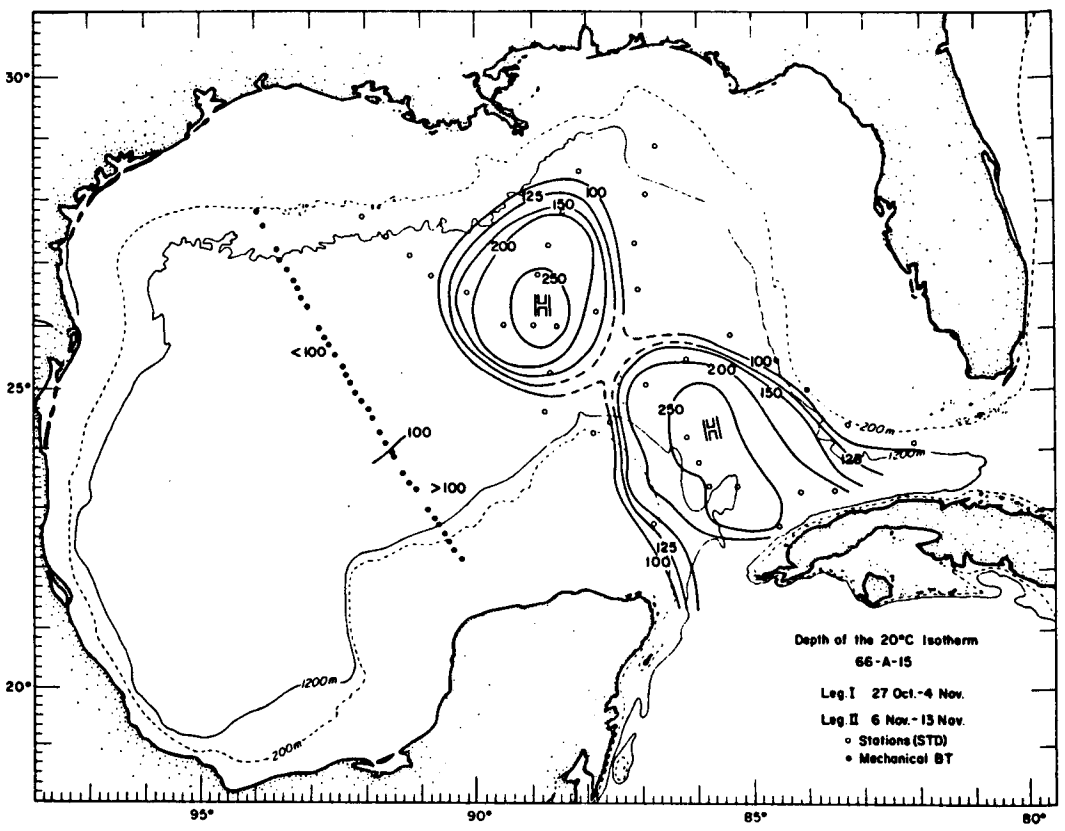

FIG. 1. Loop current eddy formation in the Gulf of Mexico (from Elliot, 1982).

3. Eddy interaction with topography and lateral boundaries

Previous studies of isolated eddies over a flat bottom (McWilliams and Flierl, 1979; Mied and Lindemann, 1979) have identified a self advective tendency for eddies associated with their nonlinear strength. This tendency arises as the eddy becomes asymmetric through dispersion of its constituent Rossby waves. Since longer wave components have greater westward phase velocities than short-wave components, dispersion favors steepening of pressure gradients on the trailing side of the eddy resulting in self advective tendency in the direction of the stronger flow there. This tendency is north (south) for cyclones (anticyclones) over a flat bottom. This self advective tendency can be in other directions for eddies which propagate over topography through topographic Rossby dispersion. In an earlier publication (Smith and O'Brien, 1983), the interaction of an isolated eddy with topography was investigated. They examined eddy propagation as influenced by: planetary β, topographic β_T and nonlinear self advective (NL) propagation tendencies. They found that anticyclones and cyclones respond differently to a topographic upslope to the west, with the response being controlled by dynamics in the lower layer. Figure 2 (from Smith and O'Brien, 1983) shows schematically these propagation tendencies.

As can be seen from the diagram for western bounding topography, anticyclones have offshore directed (eastward) NL propagation tendencies associated with nonlinear self advective tendencies which become effective after dispersive properties induce asymmetries in the eddy.

For the topography considered in Smith and O'Brien (1983) and typical of continental slope regions, β_T is two orders of magnitude greater than planetary β. A time scale for dispersive decay of an isolated vortex has been estimated in a number of ways in previous studies (Smith and Reid, 1982; Flierl, 1984; Davey and Killworth, 1984). It is generally inversely related to β, suggesting that the dispersive decay of an eddy over topography would occur on shorter time scales associated with the larger value of β_T.

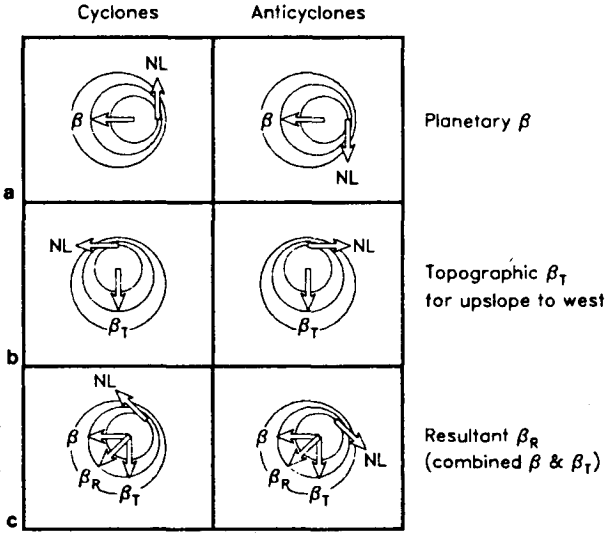

FIG. 2. Schematic propagation tendency diagram from Smith and O'Brien (1983) for a topographic upslope to the west.

As will be seen in the following numerical experiments, the motion of an anticyclone over topography can become NL dominated, whereas NL plays a secondary role in eddies over flat topography. These tendencies hold for eddies which are significantly nonlinear in the lower layer. In Smith and O'Brien (1983), eastward propagation of anticyclones occurred for a topographic slope of approximately one percent, eddy lower layer rotational velocity ($v_{2\max}$) of 0.5 m s^{-1} and eddy radius (L = 50 km) equal to the internal Rossby radius of deformation (R_d). This corresponds to a Rossby number ($\mathrm{Ro}_2 = v_{2\max}/fL$) indicative of the nonlinear strength of the eddy of order 0.1. For comparison with previous studies, a nondimensional eddy size is defined by $\gamma = L/R_d$. In Smith and O'Brien (1983) γ = 1. In this study a wider range of Ro_2 and a larger value of γ (=2) for Loop Current eddies is considered. In addition, a closer examination of the nonlinear dynamics is presented here.

The interaction of point vortices with lateral boundaries is discussed by Sommerfeld (1950). There it is shown that the interaction of a vortex with a lateral boundary is analogous to the interaction of neighboring vortices of opposite sign. Those considerations would suggest northward motion for an anticyclone adjacent to a western boundary. The nonlinear terms can also provide northward motion for anticyclones along a western boundary as shown by Cox (1979) in a study of the interaction of Somali Current eddies with a lateral no-slip western boundary. Figure 3 (from Cox, 1979) shows schematically the force vectors influencing eddy motion in those model results.

For eddies dispersing over topography, the nonlinear self advective tendencies are a function of time. For an initially strong anticyclone, offshore directed propagation can occur (Smith and O'Brien, 1983). For intermediate strength anticyclones one might anticipate a balance between the nonlinear advective tendency and the combined beta effects which would result in a stationary dispersing anticyclone over topography. As nonlinearity subsequently decreases with eddy dispersion or decay, southward (β_T controlled) motion along the topographic slope may occur by topographic Rossby wave considerations. Previous flat bottom experiments have shown that mixed mode vortices tend to evolve to upper layer features as dispersion occurs more rapidly in the lower layer. If this occurs in eddies over topography, the eddies may propagate as upper layer features independently of topography, with motion eventually controlled by the western lateral

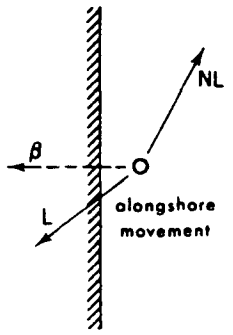

FIG. 3. Schematic diagram of L (linear), NL (nonlinear), and beta force vectors on an anticyclone impinging on a western lateral boundary (from Cox, 1979).

boundary. This would provide northward motion by the mechanisms of Sommerfeld (1950) and Cox (1979). This hypothetical sequence of events for a decaying Loop Current eddy is tested in this paper.

4. Numerical technique

Experiments are performed using a two-layer primitive equation semi-implicit numerical scheme. Motion in each layer is governed by a momentum equation:

$$\partial V_i/\partial t + (\nabla \cdot \mathbf{V}_i + \mathbf{V}_i \cdot \nabla)\mathbf{v}_i + \mathbf{k} \times f\mathbf{V}_i = -h_i \nabla P_i + A_h \nabla^2 \mathbf{V}_i \quad (1)$$

and a continuity equation:

$$\partial h_i/\partial t + \nabla \cdot \mathbf{V}_i = 0 \quad (2)$$

for layer ($i = 1$ upper and $i = 2$ lower) thickness h_i, transports $\mathbf{V}_i$ and velocities $\mathbf{v}_i$. All notation is defined in appendix A.

The scheme has been used in numerous previous studies (Hurlburt and Thompson, 1980, 1982; Smith and O'Brien, 1983) where it is more fully discussed. Linear test cases were performed for comparison with linear analytic solutions of Flierl (1977), (as discussed in Smith and Reid, 1982) providing model verification of Rossby dispersion characteristics.

Approximately 50 experiments were performed. Table 1 provides initial conditions for a representative group of these experiments. Eddy layer thickness radial distribution $h_i(r)$ is initially axisymmetric Gaussian with the velocity field in gradient balance. Eddy strength, vertical structure and friction coefficient were varied.

For most experiments, Laplacian lateral friction coefficient, A_h, was maintained at a minimal value of 100 m^2 s^{-1} for computational stability. Its role is thus thought to be minimal in damping the geostrophic scales of interest. Subgrid scale processes such as these may in fact play some role in the eventual decay of eddies over topography. Given the crudeness with which the Laplacian operator parameterizes these processes and the rapid decay times induced in eddies for large values of A_h it appears that small values are more appropriate.

The model domain is 1375 km × 975 km and is shown in Fig. 4 along with typical eddy initial condition and width of topography. Grid resolution for a given variable is 25 km. Boundary conditions are no-slip walls on the north and west and open radiation (Camerlengo and O'Brien, 1980) on the south and east. The continental slope in the northern and western Gulf between the 500 and 3500 m isobaths ranges in steepness from 10 to 30 m km^{-1}. Topography is represented by a linearly sloping bottom with slope 10.7 m km^{-1}. This slope is slightly less than that chosen in Smith and O'Brien (1983). The shallowest topography is 1500 m.

The depth of the 14°C isotherm suggests a mean upper layer thickness value of 250 m. A model constraint is that the layer interface cannot intersect the surface or bottom. Upper layer mean thickness H_1 is thus chosen to be 500 m to accommodate large interfacial distortions associated with the baroclinic structure. Lower layer mean thickness h_2 is 3000 m for all experiments. Eddy initial radius L, to maximum azi-

TABLE 1. Experiment initial conditions.

Experiment	L (km)	v_1/v_2 (m s^{-1})	$\nabla d/\nabla x$ (m km^{-1})	A_h (m^2 s^{-1})	t_{max} (days)	$\overline{Ro_2}$	γ
Mixed mode anticyclones							
LAC3	100	1.1/0.6	0	100	60	0	2.2
AC3	100	1.1/0.6	0	100	28	0.09	2.2
ACD6	100	1.1/0.6	10.7	100	60	0.09	2.2
ACD7	100	0.6/0.3	10.7	100	60	0.05	2.2
ACD8	100	0.6/0.3	10.7	100	36	0.05	2.2
ACD9	100	1.1/0.6	10.7	500	60	0.09	2.2
ACD10	100	1.1/0.6	10.7	1000	60	0.09	2.2
Multiple mixed mode anticyclones							
AC2D1	100	1.1/0.6	10.7	100	39	0.09	2.2

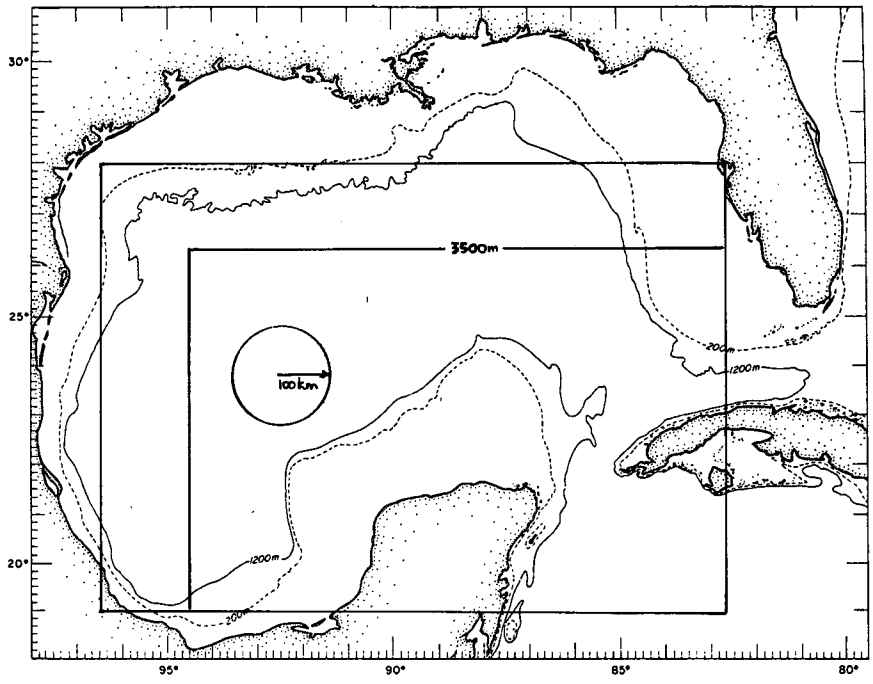

FIG. 4. Model domain and topography with eddy size (L, radius to maximum velocity = 100 km) and typical initialization location.

muthal velocity v_{max} is fixed at 100 km in all experiments. For the mean layer thickness values chosen, the first baroclinic Rossby radius is 46 km making nondimensional eddy size $\gamma = 2.2$ (twice that chosen in Smith and O'Brien, 1983).

5. Numerical experiments

The numerical experiments discussed are a subset of a larger number. Initially, a wider parameter range was explored, including parameter choices which were not realistic for Loop Current eddies. For example, pure barotropic and pure baroclinic mode initial conditions were considered. Although interesting dynamical regimes were delineated (e.g., baroclinically unstable eddies), only results appropriate to Loop Current eddies are discussed here. For "realistic" Loop Current eddy parameter choices, two robust dynamical regimes appeared in numerous experiments. A single example of each of those regimes is given below. The regimes are eddy lower layer strength dependent, with motion being controlled by lower layer dynamics for strong lower layer structure and motion being controlled by upper layer dynamics for weak lower layer flow.

a. Strong lower layer flow

Figure 5 shows time evolution of a strong anticyclone initialized adjacent to the western slope. The initial velocity shear distribution in the vertical is v_{1max}/v_{2max} = 1.2/0.6 m s^{-1}. Motion is initially southwestward consistent with flat bottom dynamics. A three-eddy pattern characteristic of many of the following experiments develops during the early portion of this experiment (Fig. 5b, day 10 and Fig. 8a). The cyclones which develop to the north and south of the original anticyclone are the separate results of the two dispersion mechanisms. The northern lower layer cyclone evolves due to topographic dispersion. The southern cyclone evolves initially to the west of the anticyclone due to planetary dispersion and is subsequently advected by the anticyclone onto topography. The mutual advection between the northern cyclone and the anticyclone gives rise to eastward propagation of the pair by day 20 with strengthening of the cyclone (through vorticity conservation) as it moves into deeper water. The fluid interface above this cyclone is depressed from its initial state, generating a weak cyclone (through vortex stretching) in the upper layer as well. Over a flat bottom, similar strengthening of a cyclone generated by planetary dispersion, does not occur since the vorticity gradient across which the vortex pair is advecting is two orders of magnitude weaker. Alternately stated in terms of vorticity conservation, large increases in layer thickness h (associated with strong cross-isobath flow into deep water) demand large relative vorticity increases, whereas weaker vorticity changes associated with latitudinal shifts in flat bottom eddies provide for weaker relative vorticity changes. A summary of eddy propagation paths (Fig. B1) and corresponding velocities (Table B1) as estimated from maximum surface height anomaly are contained in appendix B. Table B2 lists the Loop Current energetics.

The original lower layer anticyclone disperses by day 16, but the upper layer anticyclone persists for the du-

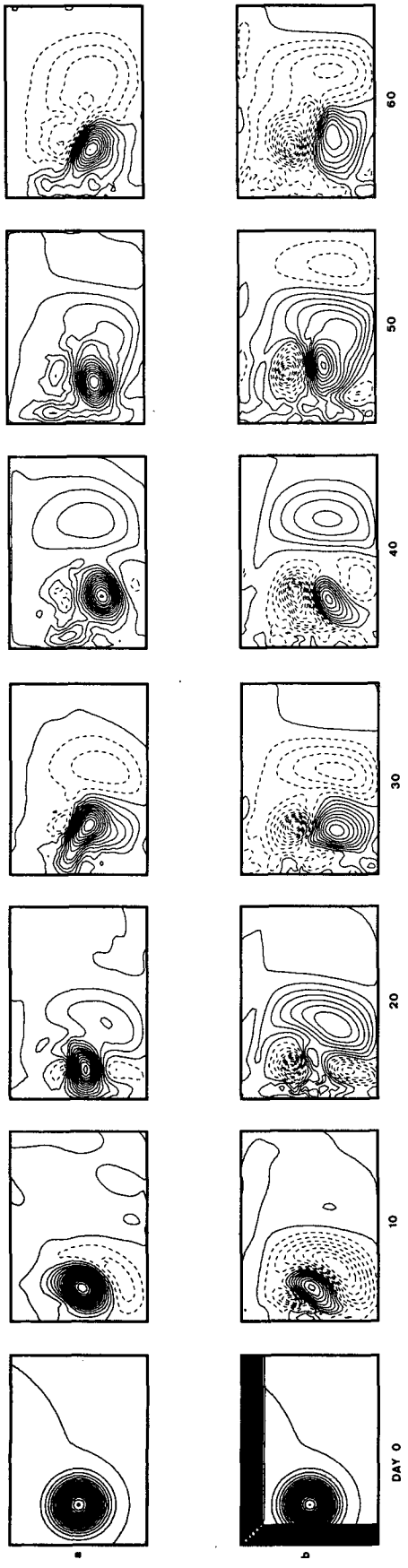

FIG. 5. Sixty-day simulation mixed mode strong anticyclone in both layers (a), (b) upper ($i = 1$), lower ($i = 2$) streamfunction ψ_i. Contour interval is 200 $m^2 s^{-1}$ for ψ_1 and 100 $m^2 s^{-1}$ for ψ_2 ACD61 = 100 km v_{1max}/v_{2max} = 120/60 cm s^{-1}.

ration of the experiment (60 days). The upper layer anticyclone trajectory for this case (Fig. 13) indicates a looping motion offshore with alternating east–west motion. Also evident (and not unrelated) is a vacillation in eddy shape from elliptical to circular.

An examination of the spatial distribution of the nonlinear terms in these eddy simulations will indicate the role they play in inducing the eddy motion. For an axisymmetric eddy in gradient balance, these terms (v^2/r in cylindrical coordinates) represent a radially outward centrifugal force (see, for example Holton, 1972). With dispersion, their distribution becomes asymmetric, with an azimuthal mode 1 (using the terminology of Olson, 1979) distribution. This distribution has a maximum value on the eastern side for planetary dispersion. This is illustrated for a flat bottom reference simulation (AC3) in Fig. 6. For eddies dispersing due to β, the orientation of this modal asymmetry is maintained as the eddy decays, so that the advective propagation tendency induced is always in the same direction (south for anticyclones). The magnitude of the centrifugal terms decays monotonically with time. As shown below this is not true for strong eddies perturbed by topography.

Figure 7 shows the maximum value of the magnitude of the advective terms (NL_{max}) as a function of time for the strong lower layer case ACD6. From the figure, lower layer NL_{max} does not decay monotonically, but reaches a maximum on day 10 in conjunction with the topographic interaction. The NL_{max} represents approximately 60 percent of the Coriolis term at this time at the same location. For dispersion induced by a topographic upslope to the west, the distribution of centrifugal forces is again skewed in an azimuthal mode-1 distribution. Dispersion is however predominantly north–south, leading to maximum values on the northern side of the anticyclone. Contours of the amplitude of the advective terms (shown in Fig. 8) show that the maximum value is located between the cyclone anticyclone pair on day 10, consistent with the topographic dispersion and the resulting mutual advection to the east.

A second period of eastward motion (see Fig. B1) occurred in the upper layer eddy beyond day 51. This eastward motion is not related to a second topographic interaction as is evidenced by uniformly decaying NL_{2max} in the lower layer (Fig. 7). It is instead related to the vacillation in radial structure in the upper layer. The westward motion (days 33–51) corresponds to a radially symmetric state followed by a second period of eastward motion in which azimuthal mode 2 structure reappears. During periods of ellipticity, the ellipse does not maintain a constant orientation but rotates anticyclonically. This mode-2 distribution is also seen in the distribution of the nonlinear terms on day 54 (Fig. 9). The strongest nonlinearity in the lower layer during the final 30 days is associated with the cyclone, not the anticyclone. The layers have become decoupled with upper layer motion dictated by self advection, but not through dispersion-generated mode 1 asymmetry.

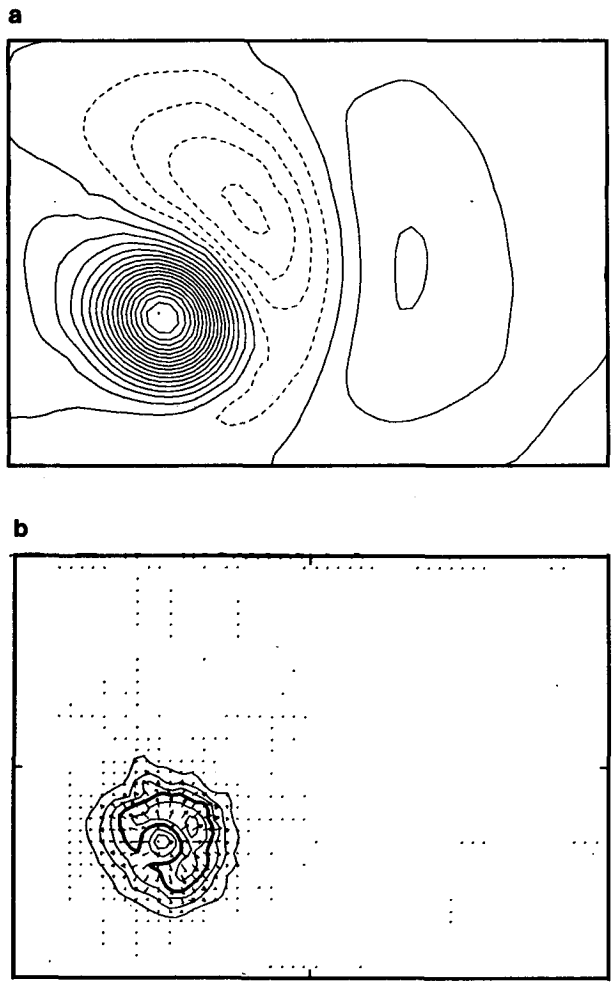

FIG. 6. Upper layer nonlinear term distribution in flat bottom case AC3. (a) upper layer stream function, day 15 (b) spatial distribution of advective terms, day 15. Amplitude distribution is contoured showing maximum values located on the trailing eastern side.

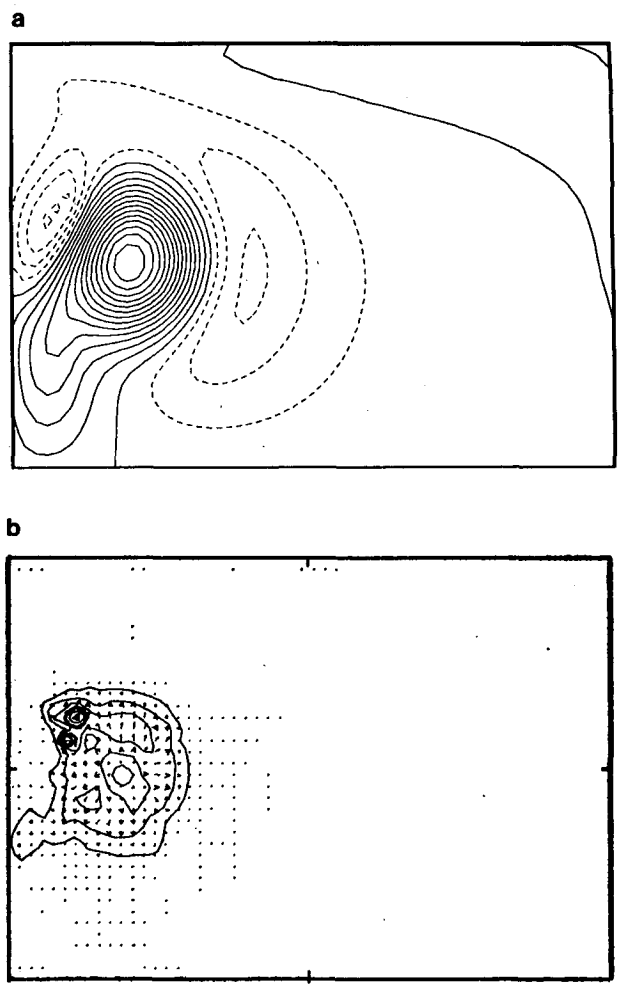

FIG. 8. Lower layer nonlinear term distribution for strong lower layer case ACD6 on day 9. (a), (b), same as Fig. 6. Contours show maximum centrifugal terms between the anticyclone cyclone pair.

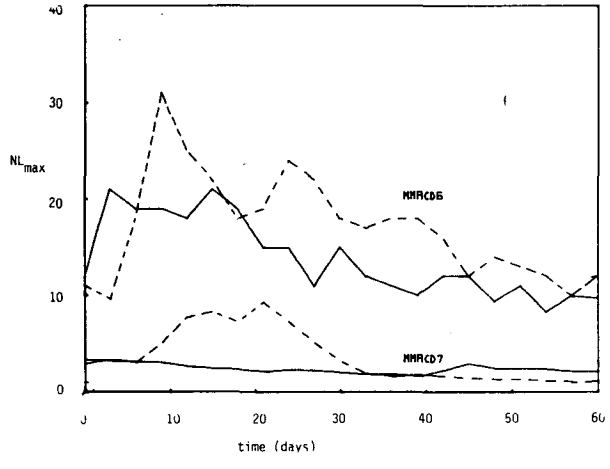

FIG. 7. Time dependence of the maximum centrifugal force NL_{max}. Upper two curves are for strong lower layer case ACD6. Lower two curves are for weak lower layer case ACD7. Lower layer NL_{max} curves are dashed.

Instead a mode-2/mode-0 vacillation is occurring. The argument of Smith and O'Brien (1983) (Fig. 2) provides a mode-1 perturbation and self advection in the direction of strongest flow. This simulation shows that mode-1 asymmetry does not persist, but that vacillation in azimuthal modal structure can provide looping motion.

Two additional experiments identical to ACD6 with the friction coefficient A_h varied to 500 and 1000 m^2 s^{-1} were performed. The NL dominated eastward propagation process is only slightly altered by an increase in lateral friction coefficient of $A_h = 500$ m^2 s^{-1}. Compare eastward propagation velocities and paths (Table B1, Fig. 13). For $A_h = 1000$ m^2 s^{-1}, the eddy is weakened rapidly such that eastward directed self advective tendencies are less effective, although still evident in propagation velocity components between days 24 and 45. This is due to the coupled effect of decreased nonlinear strength and decreased asymmetry induced by dispersion (i.e., dispersive spreading is suppressed).

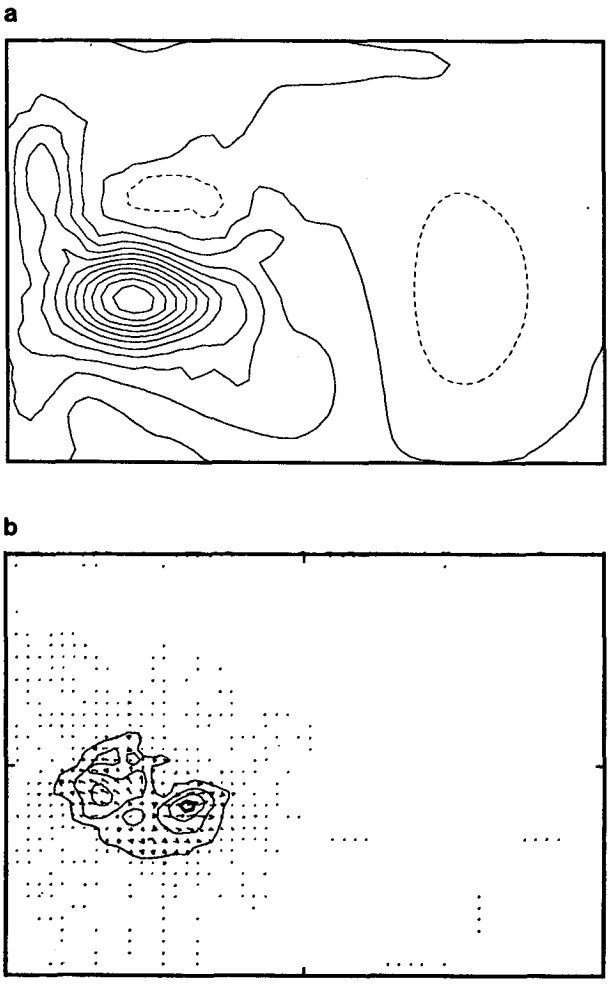

FIG. 9. Upper layer nonlinear term distribution for strong lower layer case ACD6 on day 54. (a), (b), same as Fig. 8.

Hurlburt and Thompson (1982) note the increased dispersion of eddies associated with small friction coefficient (their Experiment 4). These experiments show that eastward reflection of an anticyclone can be quantitatively altered by increased lateral frictional processes. It is not entirely suppressed however, even for A_h as large as 1000 $m^2 s^{-1}$.

These results for increased friction and those of Smith and O'Brien (1983) where smaller eddies and other vertical structures were considered, indicate that topographically induced eastward propagation of strong lower layer anticyclones is a dynamically robust result. It occurs for anticyclones when lower layer strength, Ro_2, is greater than 0.09.

b. *Weak lower layer flow*

For weaker (and probably more realistic for Loop Current eddies) flow in each layer (60/30 cm s^{-1}) the lower layer disperses rapidly during the first 18 days (Fig. 10). Upper layer motion is initially southwestward. A comparison of this simulation with a corresponding flat bottom experiment (AC3, discussed below) indicates that β_T played no significant role in inducing southward motion. The lower layer disperses so rapidly that the anticyclone becomes upper-layer controlled. Subsequent motion is northward with a translational component as large as 7 km day^{-1} induced (as will be shown) by the no-slip wall.

The spatial distribution of the nonlinear terms illustrates the asymmetry induced in the eddy by the lateral boundary (Fig. 11). Prior to day 45, the distribution of these terms resembled that seen in Fig. 6, indicative of planetary dispersion. Their distribution on day 45 however shows maximum values on the northward flowing western side of the eddy. Figure 7 shows that the maximum value was intensified, (but only slightly so) by the boundary beyond day 45. It is important to note that no significant southward motion along contours of the bottom (as would be expected from vorticity considerations for topographic Rossby waves) are observed in these simulations.

c. *Role of lateral boundaries*

In order to separate boundary effects from topography effects on eddies, the effect of a no-slip wall on flat bottom eddy motion is briefly considered here. A simulation was performed without topography and with an eddy initialized near the wall. Motion is anticyclonic in both layers (mixed mode 120/60 cm s^{-1}; L = 100 km). The propagation was initially southwest, consistent with flat bottom dynamics. In conjunction with increased Rossby number the eddy showed a stronger southward advective propagation than the case (ACD7) discussed above. Northward motion did again result through boundary-induced asymmetry. The distribution of the nonlinear terms were again as in Fig. 11, with maximum values on the northward-flowing western side. This argument for asymmetry and resulting self advection would predict southward motion for cyclones. Motion during the final 5 days of simulation is approximately 9 km day^{-1} northward. This greater northward propagation rate (than in the previous case ACD7) is also consistent with the eddy's stronger nonlinear structure.

The above simulation was repeated without the advective terms present in the numerical code. This simulation (LAC3, not shown) exhibited mostly westward motion. Only its trajectory is shown in Fig. 13.

The motion of individual anticyclones in the western Gulf is commented on briefly by Hurlburt and Thompson (1982). In their numerical simulations, they find northward motion both with and without topography. This suggests that their eddies at the time of topographic interaction fall into the weak lower layer regime here. They also note that eddies decay more slowly with free-slip boundaries.

d. *Coalescence of anticyclones*

The dynamical regime which governs an eddy's motion depends of course on the eddy's location as well

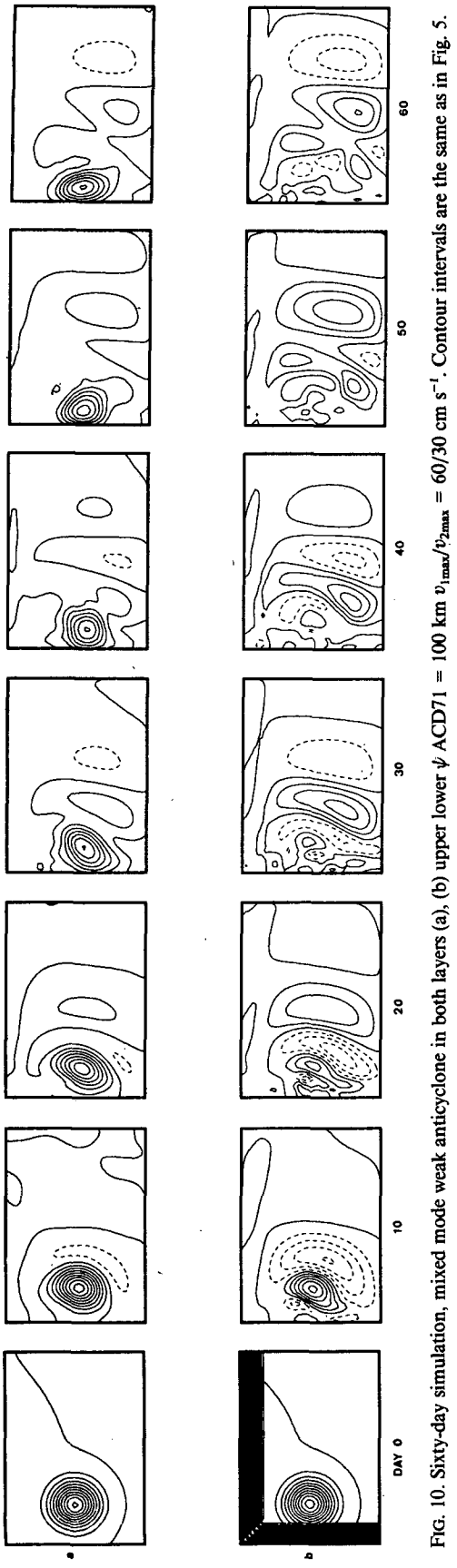

FIG. 10. Sixty-day simulation, mixed mode weak anticyclone in both layers (a), (b) upper lower ψ ACD71 = 100 km v_{1max}/v_{2max} = 60/30 cm s^{-1}. Contour intervals are the same as in Fig. 5.

as its strength. This governs the relative importance of β and β_T in Fig. 2. As previously shown, anticyclones with strong lower layer flow that interact with topography can become NL dominated, whereas NL plays a secondary role in flat bottom eddies. This suggests that adjacent anticyclones in the Gulf may have motion governed by different propagation tendencies. This motivated a coalescence experiment discussed briefly here. Could an eastward propagating NL-dominated anticyclone coalesce with a flat bottom southwestward-propagating β-dominated anticyclone?

A simulation with two mixed-mode anticyclones (not shown) provided evidence that this could occur. The eastward-propagating case ACD6 (v_{max1}/v_{max2} = 1.1/0.6 m s^{-1}) was repeated with a second identical anticyclone added offshore over the flat bottom portion of the basin.

In this experiment, the two anticyclones had oppositely-directed propagation tendencies. The western eddy (as in experiment ACD6), dominated by offshore-directed self advection after day 20, propagated into the westward β-dominated anticyclone over the flat bottom. Coincident with the coalescence on day 26 was an increase in the maximum nonlinear term (NL_{max}) in each layer, not seen in experiment ACD6 (Fig. 7). Although coalescence occurred for this particular choice of parameters, other results for single eddies here suggest that this is not a general result. For a weaker mixed mode western eddy, for example, it was shown above that eastward propagation does not occur. In addition, vertical structure appears to play some role as similar experiments (not shown) with smaller (γ = 1) but equal strength barotropic eddies failed to show coalescence. Further work is necessary to understand the dynamics of eddy coalescence and the implications for Loop Current eddies.

e. Northern slope interaction

For eddies initialized over the northern slope, topographic β_T is westward and augments westward planetary β induced motion. For realistic lower layer flows, rapid topographic dispersion occurs as in ACD7 and the remaining upper layer anticyclone propagates southwestward governed by upper layer dynamics. The trajectory for an eddy with the same characteristics as ACD7 but initialized over the northern slope (ACD8) is shown in Fig. 13. No propagation tendency exists for asymmetry induced by the lateral boundary as in experiment ACD7. This simulation suggests that Loop Current eddies which first interact with the northern continental slope before their southwestward track across the Gulf are more likely to be upper layer features, as their deep structure may be eroded by topographic dispersion.

6. Comparison with observation

The results of the numerical simulations here are in qualitative agreement with those from observations. The initial reaction of the anticyclone to topography

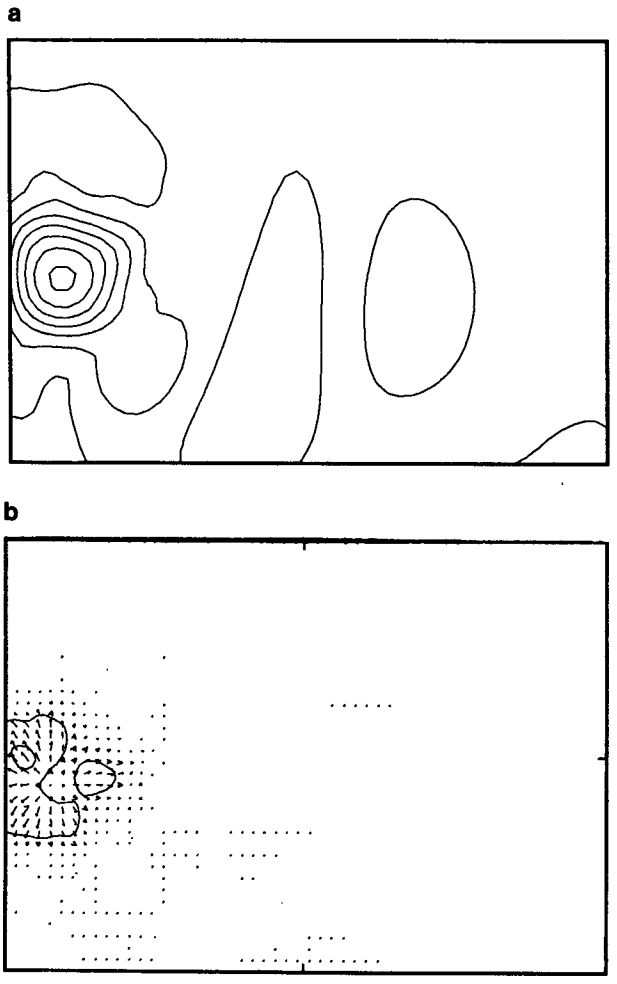

FIG. 11. Upper layer nonlinear term distribution for weak lower layer case ACD7 on day 45. (a), (b), same as Fig. 6. Contours show maximum centrifugal terms on the western side of the anticyclone.

did exhibit features observed in the western Gulf. A northern cyclone is commonly observed (Merrell and Morrison (1981); Merrell and Vasquez, 1983) as is cyclonic flow to the south (Vasquez, 1976). In simulations here, a strong cyclone evolves rapidly in the lower layer through topographic dispersion. Alternately stated, strong offshore cross-isobath flow on the northern side of the anticyclone acquires cyclonic relative vorticity as it flows into deep water. The lower layer cyclone spins up (through vortex stretching at the interface) an upper layer cyclone above it.

Detailed observations of the motion of individual Loop Current eddies in the western Gulf are limited to the drifter buoy results of Kirwan et al. (1984). The buoy tracks indicate the following propagation tendencies: An eddy which formed over the northern slope showed southwestward motion off of topography. Eddies over the flat bottom portion of the Gulf also showed southwestward propagation. Temporary eastward motion can occur after the eddies encounter topography in the western Gulf, with a subsequent generally northward motion along the Texas coast. Figure 12 shows a representative buoy track. Eddies in simulations here show southwest motion over the flat bottom portion of the domain (all simulations) prior to interaction with bottom topography. After they encounter topography, they exhibit eastward motion (case ACD6) for strong lower layer flow and northward motion (case ACD7) for weak lower layer flow.

Elliot (1982) shows trajectories for Loop Current eddies from hydrographic data. Although there are significant deviations from a mean path, he computes a mean vector of 2.1 km day^{-1} at 279°T centered along approximately 26°N. This propagation path takes the eddies along the lower portion of the continental slope in the vicinity of the 2500 m isobath. This trajectory is also occasionally seen in satellite tracked eddies (Brooks, personal communication, 1985). None of the simulations here show any tendency to follow contours of f/H in the sense of topographically-controlled waves as these observations would suggest.

No direct observations have been made of anticyclone coalescence in the Gulf of Mexico. Coalescence has been observed in other regions, however. The coalescence of anticyclones has been observed by Cresswell (1981) in the East Australian current. In that observation, two anticyclones with different water mass characteristics coalesced by an adjustment in the vertical such that a lighter eddy became located over a denser eddy.

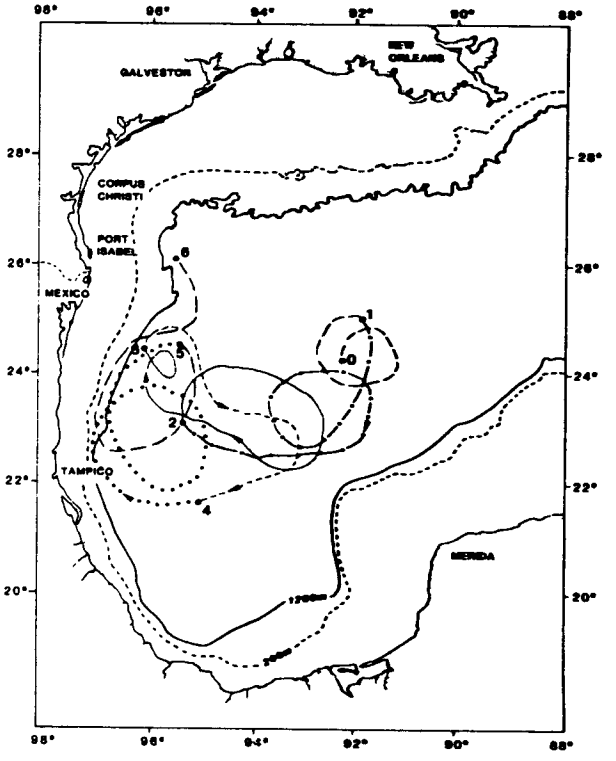

FIG. 12. Loop current eddy motion inferred from drifting buoys. (from Kirwan, et al., 1984)

7. Discussion and conclusions

The interaction of isolated Loop Current eddies with the continental slope region in the Gulf of Mexico has been examined with a two layer numerical model. Eddy asymmetry can be induced by planetary and topographic wave dispersion and eddy interaction with a lateral boundary. Asymmetry results in self advective tendencies which can dominate the motion in the latter two cases. Which of these two factors provides asymmetry in a two-layer eddy is dependent on the lower-layer rotational strength (Ro_2) of the eddy. The motion is controlled by topographic interaction for $Ro_2 = 0.09$ or greater, and motion resulting from lateral boundary interaction for $Ro_2 = 0.05$. As the eddy weakens below this value self advection no longer dominates the motion.

For strong lower layer flow, topographic dispersion promotes strong azimuthal mode 1 asymmetry, allowing nonlinear self advective effects to take the anticyclone eastward off of topography. In the process a partner cyclone (initially created by the topographic dispersion) is intensified by vortex stretching as the vortex pair moves into deeper water. This is in contrast to the suggestion by Louis and Smith (1982) that strong topography effectively linearizes eddy dynamics by increasing the characteristic phase speed relative to the particle speed (and hence promoting dispersion).

This eddy "reflection" process for strong anticyclones has unusual implications implying that cyclones and anticyclones may play different roles in western boundary current regions. Typically it is thought that western boundary regions accumulate enstrophy since reflected planetary waves at the western boundary are shorter than the incident ones (Charney and Flierl, 1981). For strongly nonlinear anticyclones however, nonlinearity inhibits dispersion tendencies and dictates reflection such that the incoming and reflected feature have similar wave number distributions.

After the anticyclone propagates away from topography, a remaining azimuthally perturbed upper layer eddy exhibits alternate east–west motion in conjunction with a vacillation between axisymmetric and azimuthal mode 2 (elliptical). Although the perturbed upper layer state is initiated by strong lower layer topographic interaction, it seems likely that eddy interaction with other features (eddies, jets or boundaries) may provide perturbed states and hence motion inconsistent with the phase propagation of planetary or topographic wave motions.

The advection of strong anticyclones away from topography is a relatively robust result. It occurs in numerous experiments (whenever $Ro_2 > 0.09$) and is not sensitive to eddy size (in the range of $\gamma = 1$–2.2), eddy vertical structure or friction (in the range of $A_h = 100$–$1000\ m^2\ s^{-1}$).

For weaker lower layer anticyclonic motion, motion becomes less controlled by topography. Results for weaker lower layer anticyclones are consistent with the above topographic linearization argument of Louis and Smith (1983). Rapid topographic dispersion erodes the lower layer structure, leaving an upper layer vortex to propagate independently of topography. The eddy motion is then dominated by interaction with the lateral boundary. The lateral boundary induces azimuthal mode 1 asymmetry with a resulting alongshore self advection tendency. The northward motion for anticyclones is consistent with considerations of point vortices (Sommerfeld, 1950) and nonlinear self advection associated with strong nonlinear terms on the western (northward flowing) side of the eddy (Cox, 1979).

Surprisingly, topographic β_T does not appear to significantly steer anticyclones along contours of f/H in either of these dynamical regimes. It instead leads to rapid erosion of eddy lower layer structure as topographic dispersion occurs on much shorter time scales than planetary dispersion. While upper layer eddy structures persist 60 days in these simulations, the lower layer distributions are (in general) eroded within the first 10 days by topographic dispersion. Thus, the observed tendency for eddies to evolve to upper layer features in flat bottom simulations is observed here, but at a more rapid rate.

A coalescence scenario for anticyclones was found. It was shown that a topographically-induced eastward-propagating (advection-dominated) anticyclone can coalesce with a westward-propagating (β-dominated) flat bottom anticyclone. Thus the semipermanence of the anticyclone–cyclone pair in the western Gulf may be related to the coalescence of Loop Current eddies.

Acknowledgments. The author would like to acknowledge the National Science Foundation for support of this work under Grant OCE-82-15489. Valuable comments on this work were received from D. A. Brooks and J. Klinck of the Department of Oceanography at Texas A&M University.

APPENDIX A

Symbols

A_h	Laplacian lateral friction coefficient
$\beta = 2.0 \times 10^{-11}$ $m^{-1}\ s^{-1}$	variation of Coriolis parameter with latitude
β_T	topographic beta
$f_0 = 0.64 \times 10^{-4}\ s^{-1}$	Coriolis parameter for mean latitude (26°N)
x, y	Cartesian coordinates directed E and N respectively
$g = 9.8\ m\ s^{-2}$	acceleration due to gravity
$g' = 0.02\ m\ s^{-2}$ $= (\rho_2 - \rho_1)^* g/\rho_1$	reduced gravity for upper, lower density ρ_i
$Ro_i = v_{imax}/fL$	Rossby number for upper ($i = 1$) lower ($i = 2$) layers
$\Delta x = 25$ km	grid spatial resolution for a given variable

$\Delta t = 5400$ s	time increment
$H_1 = 500$ m	upper layer mean thickness
$H_2 = 3000$ m	lower layer mean thickness
h_i	instantaneous layer thickness
u_0, v_0	eddy center propagation velocity components
u_i, v_i	velocities in the x, y directions
U_i, V_i	Transport in the x and y directions
$v_{i\max}$	maximum eddy rotational velocity
$L = 100$ km	radial scale to maximum azimuthal velocity $v_{\max}$
$\gamma = L/R_d$	nondimensional eddy size
$P_1 = g(h_1 + h_2 + d)$	pressure in the upper layer
$P_2 = P_1 - g'h_1$	pressure in the lower layer
$R_d = \frac{1(g'H_1H_2)^{1/2}}{f_0(H_1 + H_2)}$	first internal Rossby radius of deformation [=46 km (H_1 = 500 m)]
$c_m = -\beta R_d^2$	fastest linear Rossby wave phase speed (=3.62 km day^{-1})
NL	nonlinear self-advective tendencies
ψ_i	upper, lower layer streamfunction fields computed from $\nabla^2\psi_i = \zeta_i$
q_i	upper, lower layer potential vorticity = $(f + \zeta_i)/h_i$
ζ_i	upper, lower layer relative vorticity = $\nabla \times \mathbf{v}_i$
$d_{\min} = 1500$ m	minimum depth of topography
$t_{\max}$	duration of simulation

APPENDIX B

Summary of Eddy Propagation Paths and Corresponding Velocities and Energetics

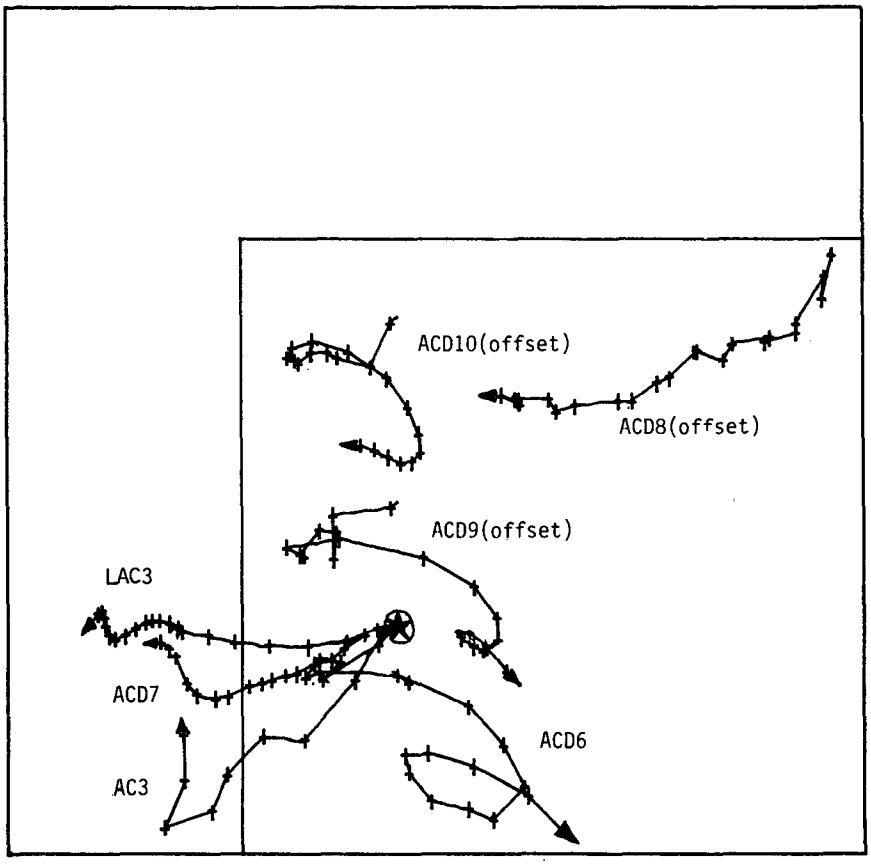

FIG. B1. Eddy trajectories based on maximum surface height anomaly. All simulations except ACD8 were initialized at the starred location. ACD8, ACD9 and ACD10 have been offset for comparison. ACD8 was initialized 438 km to the east of the location shown. Tick marks are spaced at three-day intervals.

TABLE B1. Eddy propagation speeds.

Experiment	u_0	u_0/c_m	v_0	v_0/c_m	Interval (days)	Experiment	u_0	u_0/c_m	v_0	v_0/c_m	Interval (days)
LAC3	−6.57	1.81	0.13	0.04	0–30	ACD8	−4.27	1.18	−1.42	0.39	0–33
	−1.63	0.45	−0.01	0.00	30–60	ACD9	1.47	0.41	−2.30	0.64	0–60
AC3	−8.90	2.46	−7.90	2.18	0–22		11.27	3.11	−5.0	1.38	24–39
	0.60	0.17	8.80	2.43	22–27		4.33	1.20	−3.67	1.01	51–60
ACD6	2.30	0.64	−3.17	0.88	0–60	ACD10	−3.67	1.01	−1.42	0.39	0–24
	11.68	3.23	−5.89	1.63	21–33		5.10	1.41	−3.62	1.00	24–45
	11.04	3.05	−5.79	1.60	51–60		−1.94	0.54	0.94	0.26	45–63
ACD7	−3.17	0.88	−0.24	0.07	0–60						
	−4.29	1.19	−1.95	0.54	0–21						
	−1.84	0.51	1.93	0.53	36–60						

Note: Net translation characteristics are grossly indicated by an average propagation velocity based on location of maximum surface height anomaly. Corresponding eddy trajectories are shown in Fig. B1. Dimensions of u_0, v_0 are km day^{-1}.

TABLE B2. Loop Current energetics. All energy values are normalized by 1.0×10^{13} joules.

	APE		KE_1		KE_2		BCKE		BTKE	
Experiment	I	F	I	F	I	F	I	F	I	F
LAC3	5.3	1.3	4.0	2.9	4.5	5.4	0.73	1.8	7.8	6.5
AC3	5.4	3.5	4.1	4.9	4.6	5.0	0.75	2.4	8.0	7.4
ACD6	5.3	3.3	4.0	2.7	4.5	4.4	0.73	1.7	7.7	5.4
ACD7	1.4	0.93	0.98	0.60	1.2	0.77	0.19	0.38	2.0	0.99
ACD8	1.3	1.4	0.83	0.61	0.93	0.91	0.16	0.36	1.6	1.1
ACD9	5.3	2.3	4.0	0.93	4.5	1.9	0.73	0.45	7.7	2.4
ACD10	5.3	2.2	4.0	0.62	4.5	0.69	0.73	0.42	7.7	0.89
AC2D1	11.0	9.5	8.7	5.9	9.5	11.0	1.7	2.7	17.	15.

I: initial value.
F: final value (duration of each experiment is given in Table 1).

REFERENCES

Brooks, D. A., 1983: The wake of hurricane Allen in the Gulf of Mexico. *J. Phys. Oceanogr.*, **13,** 17–129.

——, 1984: Current and hydrographic variability in the northwestern Gulf of Mexico. *J. Geophys. Res.*, **89,** 8022–8032.

——, and R. Legeckis, 1982: A ship and satellite view of hydrographic features in the western Gulf of Mexico. *J. Geophys. Res.*, **87,** 4195–4206.

Camerlengo, A., and J. J. O'Brien, 1980: Open boundary conditions in rotating fluids. *J. Comput. Phys.*, **35,** 12–35.

Charney, and Flierl, 1981: Oceanic analogues of large scale atmospheric motions. *Evolution of Physical Oceanography,* MIT Press, 620 pp.

Cox, M. O., 1979: A numerical model of Somali Current eddies. *J. Phys. Oceanogr.*, **9,** 311–326.

Cresswell, G. R., 1981: The coalescence of two East Australian Current warm core rings. *Science,* **215,** 161–164.

Davey, M. K., and P. D. Killworth, 1984: Isolated waves and eddies in a shallow water model. *J. Phys. Oceanogr.*, **14,** 1047–1064.

Dewar, W. K., 1983: Atmospheric interactions with Gulf Stream rings. Ph.D. dissertation, WHOI/MIT, 230 pp.

Elliot, B. A., 1979: Anticyclonic rings and the energetics of the circulation of the Gulf of Mexico. Ph.D. thesis, Dept. of Oceanography, Texas A&M University, 788 pp.

——, 1982: Anticyclonic rings in the Gulf of Mexico. *J. Phys. Oceanogr.*, **12,** 1292–1309.

Flierl, G. R., 1977: The application of linear quasigeostrophic dynamics to Gulf Stream rings. *J. Phys. Oceanogr.*, **7,** 365–379.

——, 1984: Rossby wave radiation from a strongly nonlinear warm eddy. *J. Phys. Oceanogr.*, **14,** 47–58.

Holton, J. R., 1972: *Introduction to Dynamic Meteorology,* Academic Press, 319 pp.

Hurlburt, H. E., and J. D. Thompson, 1980: A numerical study of Loop Current intrusions and eddy shedding. *J. Phys. Oceanogr.*, **9,** 1611–1651.

——, and ——, 1982: The dynamics of the Loop Current and shed eddies in a numerical model of the Gulf of Mexico. *Hydrodynamics of Semi-enclosed Seas,* Elsevier, 243–298.

Kirwan, A. D., W. J. Merrell, J. K. Lewis and R. E. Whitaker, 1984: Characteristics of an anticyclonic ring in the western Gulf of Mexico. *J. Geophys. Res.*, **89,** 3417–3424.

Louis, J. P., and P. C. Smith, 1982: The development of the barotropic radiation field of an eddy over a slope. *J. Phys. Oceanogr.*, **12,** 56–73.

McWilliams, J. C., and G. R. Flierl, 1979: On the evolution of isolated nonlinear vortices. *J. Phys. Oceanogr.*, **9,** 1155–1182.

Merrell, W. J., and J. Morrison, 1981: On the circulation of the western Gulf of Mexico with observations from April, 1978. *J. Geophys. Res.*, **86,** 4181–4185.

——, and A. Vasquez, 1983: Observations of changing mesoscale circulation patterns in the western Gulf of Mexico. *J. Geophys. Res.*, **88,** 7721–7723.

Mied, R. P., and G. J. Lindemann, 1979: The propagation and evolution of cyclonic Gulf Stream rings. *J. Phys. Oceanogr.*, **9,** 1183–1206.

Molinari, R. L., J. F. Festa and D. W. Behringer, 1978: The circulation in the Gulf of Mexico derived from estimated dynamic height fields. *J. Phys. Oceanogr.*, **8,** 987–996.

Olson, D. B., 1979: Frontal dynamics of a Gulf Stream ring. Ph.D. dissertation, Texas A&M University, 157 pp.

Smith, D. C., IV, and R. O. Reid, 1982: A numerical study of nonfrictional decay of mesoscale eddies. *J. Phys. Oceanogr.*, **12,** 244–255.

Smith, D. C., IV, and J. J. O'Brien, 1983: The interaction of a two layer isolated mesoscale eddy with topography. *J. Phys. Oceanogr.*, **13,** 1681–1697.

Sommerfeld, A., 1950: *Mechanics of Deformable Bodies.* Academic Press, 396 pp.

Sturges, W., and J. P. Blaha, 1976: A western boundary current in the Gulf of Mexico. *Science,* **192,** 367–369.

Vasquez, A., 1976: Currents and waters of the upper 1200 meters of the southwestern Gulf of Mexico. M.S. thesis, Dept. of Oceanography, Texas A&M University, 108 pp.